Cellulose (2018) 25:7153–7165
https://doi.org/10.1007/s10570-018-2059-x

ORIGINAL PAPER

Mechanical, thermal, and water vapor barrier properties of regenerated cellulose/nano-SiO_2 composite films

Jeevan Prasad Reddy · A. Varada Rajulu · Jong-Whan Rhim · Jongchul Seo

Received: 6 February 2018 / Accepted: 30 September 2018 / Published online: 9 October 2018

Abstract Bionanocomposite films were fabricated by reinforcing regenerated cellulose (RC) with 3-aminopropyl-functionalized silica nanoparticles (nano-SiO_2). The composite films were prepared by dissolving cotton linter RC in a 7% NaOH/12% urea solution followed by the addition of nano-SiO_2 and 5% H_2SO_4 solution. The effects of nano-SiO_2 concentration (1–5 wt% with respect to RC) on the morphology, water vapor permeability (WVP), thermal properties, and mechanical properties of the RC/nano-SiO_2 composite films were evaluated. Morphological studies indicated uniform dispersions of the low-concentration nano-SiO_2 particles in the RC matrix. The tensile strength and modulus were increased by 26% and 15%, respectively, in the presence of 2 wt% of nano-SiO_2 relative to the values of neat RC film. The WVP of the RC/nano-SiO_2 composite films decreased by 22% after reinforcement with 2 wt% nano-SiO_2. The results revealed that there is a potential interaction between RC and nano-SiO_2, resulting in improved thermal and mechanical properties of the RC/nano-SiO_2 composite films compared to those of neat RC film.

Graphical abstract Bionanocomposite films were fabricated by reinforcing regenerated cellulose (RC) with 3-amino propyl functionalized silica nanoparticles (nano-SiO_2). The effects of nano-SiO_2 (1–5 wt% with respect to RC) on the morphology, water vapor permeability (WVP), and thermal and mechanical properties of the RC/nano-SiO_2 composite films were evaluated. This study highlights the potential of organically modified nano-SiO_2 to enhance the properties of RC owing to the ability of nano-SiO_2 to interact with the RC matrix at very low concentrations (2 wt%).

J. P. Reddy · J. Seo (✉)
Department of Packaging, Yonsei University, Wonju, Gangwondo 26493, Republic of Korea
e-mail: jcseo@yonsei.ac.kr

A. Varada Rajulu
Centre for Composite Materials, International Research Centre, Kalasalingam University, Anand Nagar, Krishnan Kovil 626126, India

J.-W. Rhim
Center for Humanities and Sciences, Bionanocomposite Research Center, Department of Food and Nutrition, Kyung Hee University, Seoul 02447, Republic of Korea

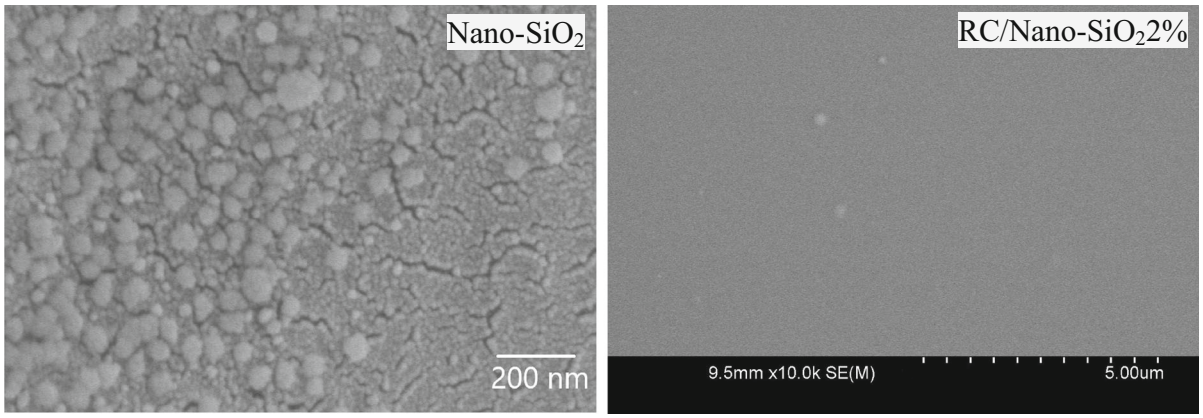

Keywords Composites · Nano-SiO_2 · Biodegradable polymer · Regenerated cellulose · Interaction

Introduction

Recently, the use of biopolymers has become widespread for food packaging because of increasing environmental complications inflicted by non-biodegradable polymers. The ability of protein- and carbohydrate-based biopolymers to form films and their potential application in food packaging has already been demonstrated (Tang et al. 2012). Cellulose is the most promising biodegradable polymer because of its abundance in ligno-cellulosic waste. Cellulose is a linear polymer comprising β-1,4-glucopyranose monomeric units (Moon et al. 2011).

Cellulose has been used to prepare composites and nanocomposites due to its unique nature. Cellulose is extensively used as a reinforcing material, particularly as nanofiller, because of its low-cost (Khalil et al. 2012). Furthermore, it is considered a nearly inexhaustible raw material that can meet the increasing demand for developing environmentally friendly and biocompatible products (Klemm et al. 2005). However, the application of cellulose as a matrix is limited because of its insolubility and poor film-forming ability. In recent years, a simple method has been developed using harmless and low-cost chemical reagents to produce regenerated cellulose (RC) materials without generating any hazardous byproducts. It involves the dissolution of cellulose in aqueous NaOH/urea or LiOH/urea solutions at low temperatures, followed by the regeneration of cellulose (Yang et al. 2011; Cai et al. 2007a). These solvents can readily dissolve even highly crystalline cellulose without causing significant degradation. New cellulose-based multifilament fibers (Cai et al. 2007b) and films (Qi et al. 2009) have been prepared from cellulose dopes. Moreover, several investigations have been made to improve the properties of RC films to increase their efficacy as packaging materials. Nadhan et al. (2012) fabricated green composite films of short waste silk fibers and cellulose by dissolving cellulose in aqueous solutions (mixture of 7 wt% NaOH and 12 wt% urea) containing different amounts (1–5%) of short silk fibers to improve the mechanical properties of RC films. *Sterculia urens* short fibers were also used to reinforce RC films; the films showed enhanced mechanical, thermal, and biodegradation properties (Jayaramudu et al. 2013). Ashok et al. (2015) used alkali-treated short fibers of a newly identified plant, *Thespesia lampas*, as fillers to reinforce RC films.

Recently, nanofillers rather than macroscale fillers have attracted attention for improving the properties of biopolymers. RC nanocomposite films have been studied by several researchers. Mahmoudian et al. (2012) prepared montmorillonite (MMT) nanoclay/RC nanocomposite films and reported that the tensile strength and Young's modulus of the RC films were improved by 12% and 40%, respectively, with the addition of 6 wt% MMT and that the films exhibited improved gas barrier properties and water absorption resistances compared to those of cellulose films. RC nanocomposite films incorporating zeolites at different concentrations showed significantly improved

mechanical properties compared to pure RC films (Soheilmoghaddam et al. 2014). Further, carbon nanotubes (Kim et al. 2010; Rahatekar et al. 2009; Zhang et al. 2007), graphite oxides (Han et al. 2011), nano-carbon black (Zhang et al. 2006), and nanohydroxyapatite (Tsioptsias and Panayiotou 2008) were also used to enhance the properties of RC films.

Among various nanofillers, silica nanoparticles (nano-SiO_2) are considered very promising materials because of their low densities, good mechanical and thermal stabilities, and chemical inertness (Boissiere et al. 2001; Grun et al. 1997; Thomas et al. 2003). Polymer nanocomposites using nano-SiO_2 particles have received much attention from several research groups in recent years (Zou et al. 2008). Unmodified solid nano-SiO_2 particle-reinforced RC films have already been reported (Song and Zheng 2013). However, they used microcrystalline cellulose and dissolved the cellulose in ionic liquids to obtain RC. The results indicated significant improvements in mechanical properties only at 7 wt% nano-SiO_2 content. Therefore, in the present study, we have focused on relatively low contents of nano-SiO_2 dispersed in water and blended with cotton linter RC in low-cost NaOH/urea solutions. To the best of our knowledge, cotton linter RC/nano-SiO_2 composite films have not been reported to date. In addition, it is well known that solid nano-SiO_2 particles tend to agglomerate when they are in water because of hydrogen bonding of the surface hydroxyl groups of nano-SiO_2. This agglomeration can result in poor dispersibility of nano-SiO_2 in polymer matrices and affect physical properties such as the mechanical strength, thermal stability, and transparency of the derived nanocomposites (Lai and Hsieh 2016). Therefore, functionalized nano-SiO_2 has been used to prevent agglomeration when used to reinforce RC matrices (Yan et al. 2007; Zhu et al. 2010). Hence, we used 3-aminopropyl-functionalized nano-SiO_2 to enhance the compatibility between RC and nano-SiO_2. The 3-aminopropyl-functionalized nano-SiO_2 particles can be well dispersed in water and are expected to be more compatible with the RC matrix than unmodified nano-SiO_2.

The main objective of the present work was to use 3-aminopropyl-functionalized nano-SiO_2 as reinforcing agents to enhance the physical properties of RC film. Therefore, the effects of nano-SiO_2 on the mechanical, thermal, and water vapor barrier properties of the RC composite films were evaluated.

Materials and experimental methods

Materials

Cotton linter pulp supplied by Hubei Chemical Fiber Co., Ltd. (Xiangfan, China) was used as received. The 3-aminopropyl-functionalized nano-SiO_2 (size: < 50 nm), sodium hydroxide (NaOH), urea, and sulfuric acid (H_2SO_4) were purchased from Sigma Aldrich, India.

Preparation of RC/nano-SiO_2 composite films

The films were prepared following a method reported by Cai et al. (2007a). Firstly, NaOH (7 g) and urea (12 g) were dissolved in distilled water (81 mL) in a 250-mL beaker and cooled to − 12 °C. To this, cotton linter (4 g) was added and stirred vigorously with a mechanical stirrer for 2 min to dissolve the cellulose. The cellulose solution was centrifuged at 7200 rpm for 20 min at 5 °C. The precipitate containing undissolved cellulose was discarded; only the decant was used for further work. The transparent solution of cellulose was mixed with nano-SiO_2 particles in a beaker, using a mechanical stirrer for uniform distribution. The nano-SiO_2 content was varied from 1 to 5% (w/w of cellulose). Then, the RC/nano-SiO_2 composite mixture was sonicated using an ultrasonic bath sonicator (Effem Technologies Ltd., New Delhi, India) for 30 min. Subsequently, 20 mL of the solution was poured onto a glass plate and spread evenly using a glass tube to obtain uniform films. The films were subsequently regenerated in a 5% H_2SO_4 solution for 5 min by dipping the plate and then stored in deionized water for 24 h. The composite films were then fixed on a polyvinyl chloride (PVC) sheet to avoid wrinkling and dried at 27 °C. The dried films were peeled from the PVC sheet and conditioned in a constant-temperature humidity chamber set at 25 °C and 50% relative humidity (RH) for at least 48 h, before further tests. The average film thickness was measured at five random positions of the film using a micrometer (Dial Thickness Gauge 7301, Mitutoyo Co. Ltd., Kawasaki, Japan) with an accuracy of 0.01 mm.

Chemical structure and transparency

To characterize the chemical structure of RC and RC/nano-SiO_2 composite films, Fourier-transform infrared (FT-IR) spectra were recorded on a Spectrum 65 FT-IR spectrometer (Bruker, Germany) from 400 to 4000 cm^{-1} in an attenuated total reflection (ATR) mode. The film transparency was measured using a UV/visible spectrophotometer (Model UV5, Mettler Toledo International Inc., Columbus, OH, USA). The transmittance at a wavelength of 660 nm (T_{660}) was measured and the average values were reported.

Morphology

The morphologies of nano-SiO_2, RC, and RC/nano-SiO_2 composite films were observed using a field-emission scanning electron microscope ((FE-SEM, S-4800, Hitachi Co., Ltd., Matsuda, Japan.) operated at an acceleration voltage of 10 kV and current of 10 μA. The nano-SiO_2 sample was prepared by dropping nano-SiO_2 suspension onto a 300-mesh nickel grid and drying at 25 °C; the morphology of the nanoparticles was observed in the transmission mode. The diameters of the nano-SiO_2 particles were measured at different points using the internal scale of the instrument and averaged. The RC film and RC/nano-SiO_2 composite films were coated with osmium using a vacuum sputter coater before testing. The presence of Si was determined by SEM- EDS analysis using Jeol SEM (JSM IT 300, USA) instrument.

Water vapor permeability (WVP)

The water vapor permeability (WVP) of RC and RC/nano-SiO_2 films were gravimetrically determined according to ASTM E96-97 with some modifications (Gennadios et al. 1994). A poly(methyl methacrylate) cup with an average depth of 2.5 cm and interior diameter of 6.8 cm was used to measure WVP. Films were cut into squares (7.5 cm × 7.5 cm) and mounted on the top of the cups containing 18 mL of water. Each film was tightened over the cup using screws to prevent leakage of water vapor. The entire cup was weighed and subsequently placed in a humidity chamber set at 25 °C and 50% RH. The weight loss of each cup was measured at intervals of 1 h over a period of 8 h. The slopes of the steady-state (linear) portion of the weight loss versus time curves were used to calculate the water vapor transmission rate (WVTR; g/m^2 s) of the film. Then, the WVP (g m/m^2 s Pa) of the film was calculated as follows:

$$\mathrm{WVP} = (\mathrm{WVTR} \times L)/\Delta p, \quad (1)$$

where L is the mean thickness of the film and Δp is the partial water vapor pressure difference (in Pa) across the film. Five measurements were made for each sample and averaged.

Water contact angle (CA)

The surface hydrophobicity of the RC/nano-SiO_2 composite films was determined by measuring the water contact angle (CA) of the film surface using a CA analyzer ((Phoenix 150, Surface Electro Optics Co., Ltd., Kunpo, Korea). For this, the films were cut into rectangular strips (3 cm × 10 cm) and directly placed on the horizontal movable stage (black Teflon-coated steel, 7 cm × 11 cm) fitted with the CA analyzer. A drop of water (ca. 10 μL) was placed on the film surface using a micro syringe. The CAs on both sides of the water droplet were measured to assume symmetry and horizontal level. Five measurements were made for each sample and the averaged values were presented in degrees.

Moisture content (MC)

The moisture content (MC) of the RC film and RC/nano-SiO_2 composite films was determined using a drying oven method (Rhim and Wang 2013). The rectangular films were cut into 3 cm × 3 cm squares and subsequently dried at 105 °C for 24 h in an oven. The MC was calculated from the weight loss and is expressed as % MC.

Tensile properties

The tensile properties of the RC/nano-SiO_2 composite films were determined per ASTM D 882-02. Specimens with dimensions of 100 mm × 10 mm × 0.03 mm were chosen. The tensile properties such as the maximum stress, Young's modulus, and elongation (%) at break were determined using a universal testing machine (INSTRON 3369, Illinois Tool Works Inc., Glenview, USA) at a crosshead speed of 5 mm/min by maintaining a gauge length of 50 mm. In each case, 15

samples were tested at 50% RH and 23 °C and the averaged values of these measurements were reported.

Thermal properties

Thermogravimetric analysis (TGA) of RC film and RC/nano-SiO_2 composite films were performed using an SDT Q600 analyzer (TA Instruments Co., New Castle, USA) under a nitrogen atmosphere. The samples were scanned from 30 to 600 °C at a heating rate of 10 °C/min.

Differential scanning calorimetry (DSC) of the RC film and RC/nano-SiO_2 composite films were performed using an SDT Q600 analyzer (TA Instruments Co., New Castle, USA) instrument under nitrogen. The initial sample weight was 5–8 mg for each specimen. The specimen was heated from 30 to 600 °C at a heating rate of 10 °C/min.

Statistical analysis

Depending on the analysis, different numbers of samples were measured individually and the mean value with a standard deviation (SD) was reported. The statistical analysis was performed by one-way analysis of variance (ANOVA), using the SPSS computer program for Windows (SPSS Inc., Chicago, USA). The significance of every mean property value was measured ($p < 0.05$) with the Duncan's multiple-range test.

Results and discussions

Chemical structure and transparency

FT-IR

FT-IR spectroscopy was used to characterize the chemical interactions between RC and nano-SiO_2 particles. Figure 1 shows the absorption for 3-amino-propyl-functionalized nano-SiO_2 particles at $\sim$ 2928 cm^{-1} (C–H stretching), which indicates the presence of –CH_2 groups (Pasternack et al. 2008). The peak at $\sim$ 1605 cm^{-1} (N–H bending) indicates the presence of –NH_2 groups. The broad peak at 3500 cm^{-1} corresponds to the stretching vibrations of O–H groups present in nano-SiO_2. The bands at 466 cm^{-1} correspond to the Si–O–Si bending vibration. Further, the sharp peaks observed at about 812 cm^{-1} and 1093 cm^{-1} are related to the symmetric and antisymmetric stretching vibration modes of Si–O–Si, respectively (Zha et al. 2015). The 3-amino-propyl functionalization was performed to avoid immediate agglomeration of the nano-SiO_2 in water. This avoids the formation of agglomerates, promoting the interaction of nano-SiO_2 with the RC matrix compared to that by unmodified nano-SiO_2.

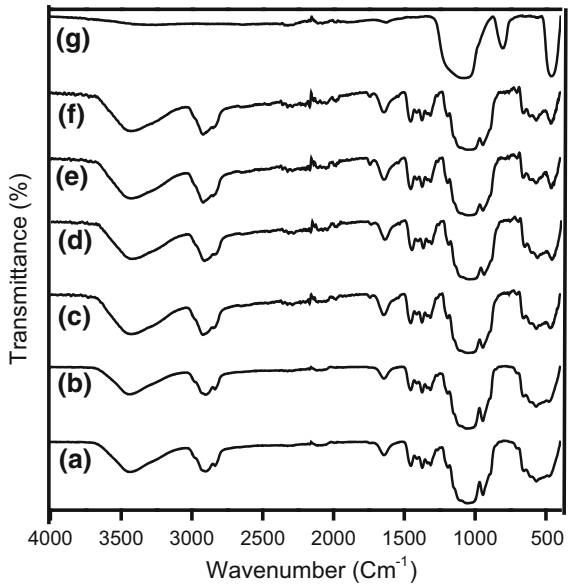

Fig. 1 FTIR spectra of RC film and RC/nano-SiO_2composite films (a) RC, (b) 1% nano-SiO_2, (c) 2% nano-SiO_2, (d) 3% nano-SiO_2, (e) 4% nano-SiO_2, (f) 5% nano-SiO_2 and (g) nano-SiO_2

As shown in Fig. 1, the neat RC film and all the composite films exhibit several absorption peaks at approximately 3456 cm^{-1}, 2903 cm^{-1}, 1640 cm^{-1}, and 1376 cm^{-1}, corresponding to the O–H stretching vibration, the C–H stretching vibration, the –OH stretching vibration, and the O–H bending vibration in RC, respectively (Li et al. 2012). In the case of RC/nano-SiO_2, the peak observed at 763 cm^{-1} corresponds to Si–O–C stretching (Dai et al. 2015). This result indicated that the OH groups present in nano-SiO_2 react with the cellulose hydroxyl to form Si–O–C. A reaction mechanism assumed based on the FT-IR results is given schematically below (Scheme 1).

Transmittance

As shown in Table 1, the RC film is visibly transparent with a transmittance of 91.2% at 660 nm. Depending

Scheme 1 Schematic for the reaction of RC/nano-SiO_2 films

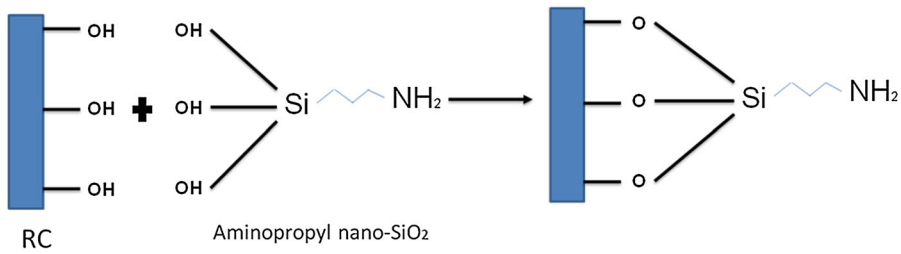

Table 1 Transparency and mechanical properties of RC and RC/nano-SiO_2 composite films

Sample code	Thickness (μm)	T^1_{660} (%)	TS2 (MPa)	EM[3] (GPa)	EB[4] (%)
RC	25.5 ± 0.8^{a}	91.3 ± 1.2^{e}	73.4 ± 3.1^{b}	5.5 ± 0.11^{ab}	5.1 ± 0.2^{e}
RC/nano-$SiO_2$1%	27.1 ± 1.3^{b}	87.5 ± 1.3^{d}	84.1 ± 3.8^{c}	6.1 ± 0.21^{c}	4.5 ± 0.3^{d}
RC/nano-SiO_2 2%	31.6 ± 0.7^{c}	86.5 ± 0.7^{d}	95.1 ± 2.5^{d}	6.7 ± 0.13^{c}	2.6 ± 0.2^{c}
RC/nano-SiO_2 3%	33.6 ± 1.4^{d}	82.4 ± 1.5^{c}	85.3 ± 2.5^{c}	6.1 ± 0.07^{d}	2.3 ± 0.1^{b}
RC/nano-SiO_2 4%	36.0 ± 1.1^{e}	79.3 ± 0.9^{b}	73.4 ± 3.1^{b}	5.6 ± 0.11^{b}	2.1 ± 0.1^{b}
RC/nano-SiO_2 5%	36.5 ± 1.6^{e}	73.6 ± 1.1^{a}	36.5 ± 1.8^{a}	5.4 ± 0.12^{a}	1.6 ± 0.1^{a}

Each value is the mean value with the standard deviation. Any two means in the same column followed by the same letter are not significantly ($p > 0.05$) different by Duncan's multiple range test

[1]Transmittance (%) at 660 nm

[2,3,4]Tensile strength, elastic modulus, and elongation at break, respectively

on the SiO_2 content, the composite films show relatively good transmittance in the range 73–87%, indicating good and homogeneous dispersions of the nano-SiO_2 in RC. However, the transmittance values are decreased linearly with increases in the nano-SiO_2 content. The decrease in transmittance of the RC/nano-SiO_2 composite films is attributed to the obstruction of light passage by the opaque nano-SiO_2 particles and agglomeration at high contents of nano-SiO_2, as described in the SEM analysis.

Morphology

The SEM image of the nano-SiO_2 (Fig. 2a) shows spherical particles with diameters of 20–40 nm. To understand the dispersibility of nano-SiO_2 particles in the cellulose matrix, the surface morphologies of the RC film and RC/nano-SiO_2 composite films with 2 and 5 wt% nano-SiO_2 are observed by SEM, as shown in Fig. 2. The neat RC film (Fig. 2b) shows a very smooth surface. However, at 2 wt% loading, the nano-SiO_2 particles are observed to be uniformly dispersed in the RC matrix (Fig. 2c, d). This implies that nano-SiO_2 has a strong affinity for the RC biopolymer because of its functionalization, enabling uniform dispersion, which may lead to higher strength and stiffness compared to those of the neat RC film. The composite film with 5 wt% nano-SiO_2 shows a rough surface with some apparent nano-SiO_2 particle agglomeration (Fig. 2e, f). This is because of the non-uniform dispersion of nano-SiO_2 in the RC matrix; the film is expected to exhibit poor mechanical properties compared to that with a relatively lower nano-SiO_2 content.

Further, elemental mapping was performed to detect silicon using energy-dispersive X-ray spectroscopy (EDS) analysis. Figure 3 shows the individual elemental maps of RC/nano-SiO_2 films. These maps reveal that C, and Si are the elemental constituents of the RC/nano-SiO_2 film. Further, the elemental map of Si suggests a homogeneous dispersion of nano-SiO_2 nanoparticles in the RC matrix at low concentrations (2%).

Tensile properties

The measured tensile properties of the neat RC film and RC/nano-SiO_2 composite films with different

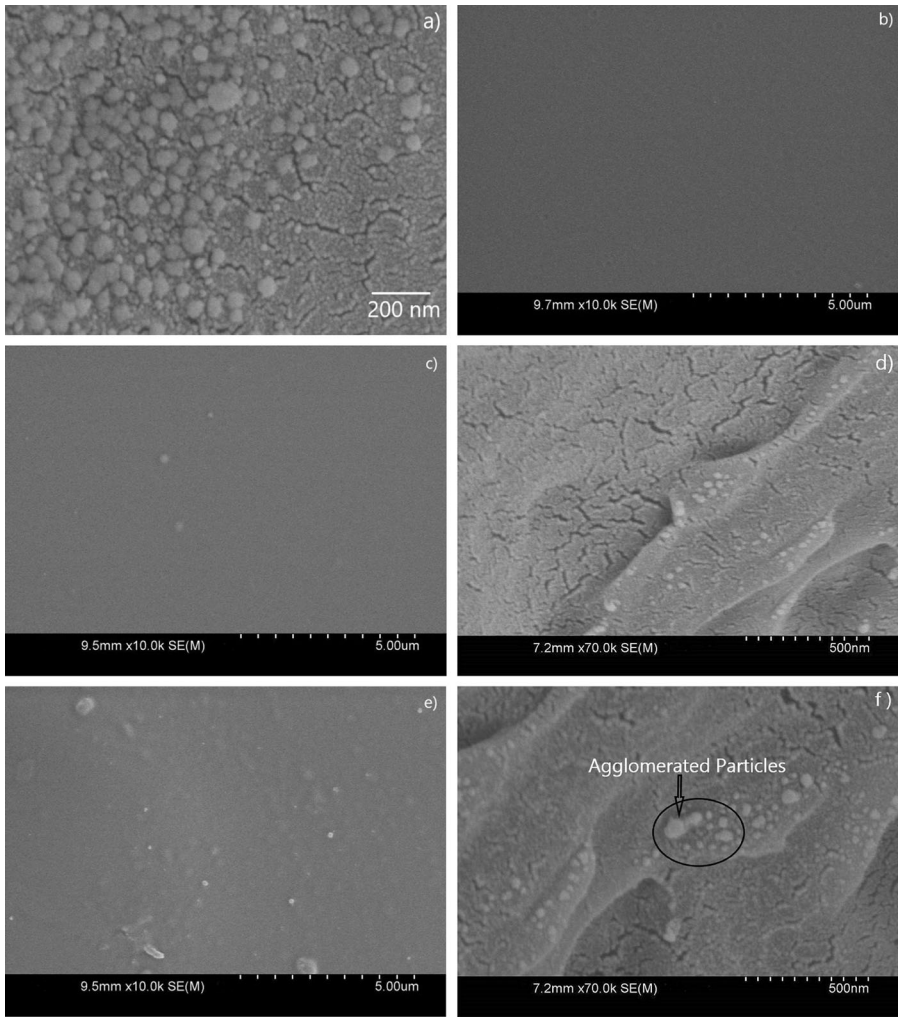

Fig. 2 SEM images of **a** nano-SiO_2, **b** RC film, **c**, **d** RC/nano-SiO_2 2% film, and **e**, **f** RC/nano-SiO_2 5% film

nano-SiO_2 contents are summarized in Table 1. The film thickness is increased linearly with the increase in the content of nano-SiO_2 mainly because of the increase in the solid content. The tensile properties of the composite films, such as the tensile strength, stiffness, and flexibility, as determined by their tensile strength (TS), tensile modulus (TM), and elongation at break (EB), respectively, are changed significantly compared to those of the neat RC film. Further, the variation is strongly dependent on the nano-SiO_2 content. The TS of the RC film is increased by 26% from 73.4 to 95.1 MPa with 2 wt% nano-SiO_2 incorporation. A similar trend is observed for the stiffness of the nanocomposite films, i.e., their TM values. The highest TM is observed for the composite film incorporating 2 wt% nano-SiO_2, with a 14% improvement in the toughness as compared to neat RC film. The improvement in the TS and TM of the composite films is attributed to the good dispersion of nano-SiO_2 in the RC, as observed in the SEM images (Fig. 1). However, the TS and TM of the composite films are decreased at higher concentrations of nano-SiO_2 (> 2 wt%). At higher concentrations, the nano-SiO_2 particles might be agglomerated (Fig. 1c) in the polymer matrix, thereby causing the attenuation of the strength and modulus. This is consistent with the results reported by Bikiaris et al. (2005), in which agglomeration caused the deterioration of mechanical properties, particularly when the aggregate sizes were increased by increased nanofiller content.

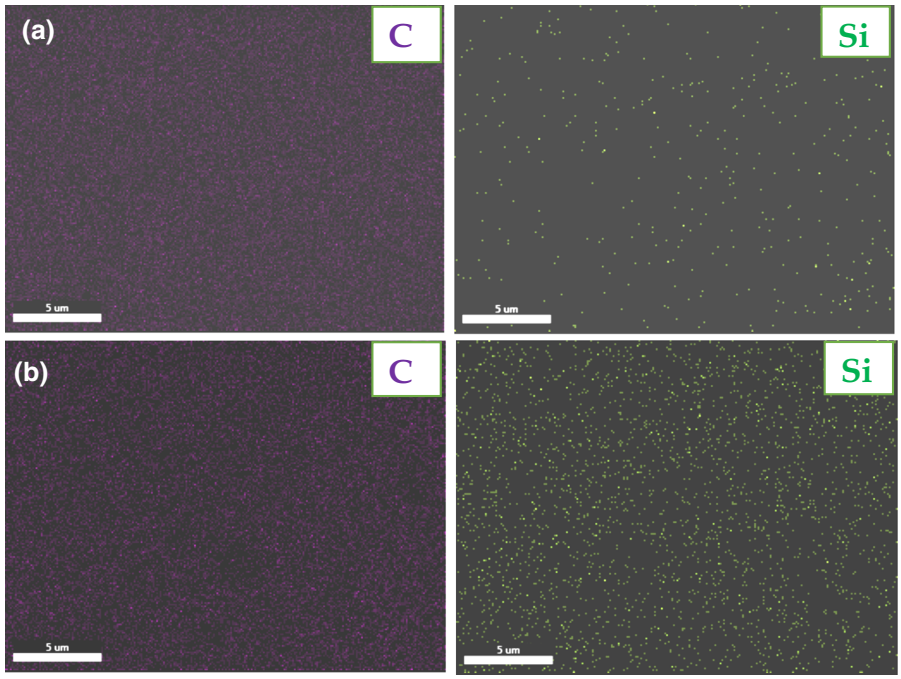

Fig. 3 Elemental mapping images of **a** RC/nano-SiO_2 2% film, and **b** RC/nano-SiO_2 5% film [green dots indicates Si]. (Color figure online)

Agglomerated nanoparticles in the polymer matrix induce uneven stress transfer between the matrix and filler, resulting in deteriorated mechanical properties.

On the contrary, the flexibility as measured by the EB of the composite films is decreased significantly compared to that of neat RC film, and the EB is constantly decreased with increase in nano-SiO_2 content. The decreased flexibility of the composite films upon blending with fillers is a commonly observed phenomenon in polymer composites (Vladimirov et al. 2006). The EB of a nanocomposite film is generally influenced by the volume fraction of the added nanofiller, its dispersion in the matrix, and the interaction between the nanofiller and the matrix. The reduction in EB value implies that the ductility of neat RC decreases in the presence of relatively rigid nano-SiO_2 and with increase in filler content.

The mechanical strengths of the RC/nano-SiO_2 nanocomposite films were compared with those of other nanoparticle-reinforced RC films reported previously, as presented in Table 2. From this table, it can be observed that the tensile properties (strength and modulus) of RC composite films with modified nano-SiO_2 are higher than those of other nanocomposite films. Further, it can be observed that the tensile properties of nanocomposite films with modified nano-SiO_2 are higher than those of films with unmodified SiO_2, even at low concentrations (2%).

Water vapor permeability (WVP)

The variations in WVP with the nano-SiO_2 content in the RC/nano-SiO_2 composite films are presented in Table 3, along with the WVP of RC film. The WVP of RC film shows a strong dependence on the content of nano-SiO_2 ($p < 0.05$). The WVP decreases with the increase in nano-SiO_2 content up to 2 wt%, and then increases slightly. The maximum reduction in WVP is observed in the RC/nano-SiO_2 composite film blended with 2 wt% nano-SiO_2. This result is in good agreement with those previously reported for cellulose/nanoclay composite films (Farahani et al. 2015). It is well known that the WVP of similar nanofiller-reinforced composite films are decreased because of the increasingly tortuous paths for vapor diffusion caused by the impermeable nanofillers (Lagaron et al. 2004). Reddy and Rhim (2014) reported that the presence of the nanofiller increased the tortuous path

Table 2 Comparison tensile properties of regenerated cellulose nanocomposite films

Source of cellulose	Solvents	Cellulose Wt (gm)	Nanomaterials (%)	Tensile strength	Tensile modulus	Elongation (%)	References
Cotton linters	NaOH/ urea	4	CNT (2%)	84.9	3.0	11.1	Qi et al. (2013)
Microcrystalline cellulose	BMIMCl	8	MMT(15%)	67	2.6	6	Mahmoudian et al. (2012)
MCC	NaOH/ urea	4	Graphite oxide (7.5%)	83.1	1.91	5	Han et al. (2011)
MCC	BMIMCl	6	Sepiolite (6%)	61.6	3.5	7.1	Mohammad et al. (2014)
Microcrystalline cellulose	BMIMCl	6	Halloysite nanotube (6%)	49.1	3.4	8.6	Mohammad et al. (2013)
Microcrystalline cellulose	AMIMCl	5	Nano-SiO_2 (7%)	76.8	–	5	Song and Zheng (2013)
Cotton linters	NaOH/ urea	4	Modified nano-SiO_2 (2%)	95.1	6.7	2.6	Present work

Table 3 Water vapor permeability (WVP), moisture content (MC), and contact angle (CA) in RC film and RC/nano-SiO_2 composite films

Sample code	WVP ($\times 10^{-9}$g m/m^2 Pa s)	MC (%)	CA (degree)
RC	2.28 ± 0.06^{e}	15.4 ± 0.15^{b}	45.9 ± 1.0^{a}
RC/nano-$SiO_2$1%	1.91 ± 0.01^{d}	14.4 ± 0.52^{ab}	47.1 ± 1.7^{a}
RC/nano-SiO_2 2%	1.62 ± 0.01^{a}	13.8 ± 0.14^{a}	49.7 ± 0.4^{b}
RC/nano-SiO_2 3%	1.79 ± 0.01^{b}	14.3 ± 0.27^{ab}	46.2 ± 1.7^{a}
RC/nano-SiO_2 4%	1.86 ± 0.02^{c}	13.6 ± 1.21^{a}	46.4 ± 1.3^{a}
RC/nano-SiO_2 5%	1.94 ± 0.01^{d}	14.6 ± 0.32^{ab}	46.3 ± 1.5^{a}

Each value is the mean of three replicates with the standard deviation. Any two means in the same column followed by the same letter are not significantly ($p > 0.05$) different by Duncan's multiple range test

length of water vapor diffusion in agar-based films, leading to decreased WVP.

In the present case, the reduction in WVP of nano-SiO_2 is attributed to the inherent barrier property of nano-SiO_2. The high-surface-area nano-SiO_2 blocks and/or traps moisture molecules; surface silanol and aminosilane groups form hydrogen bonds with both water and RC (Saravanan et al. 2016). Because of this effect, the water molecules present in the film show increased dwell times. When moisture diffuses through the film, the water molecules initially form hydrogen bonds with the nano-SiO_2/RC interfaces, following a trend similar to that for 1–3 wt% nano-SiO_2 loaded films. However, the WVP of the RC/nano-SiO_2 composite film with higher contents of nano-SiO_2 (4 and 5 wt%) is increased compared to those of films with 2 wt% or 3 wt% nano-SiO_2. Again, this could be attributed to the agglomeration of nano-SiO_2 particles when incorporated at higher concentrations, as shown in the SEM images. The agglomerated nanoparticles have more particle–particle interactions, rather than forming hydrogen bonds with the diffusing water molecules. As a result, the water molecules can easily diffuse through the RC film in which the nano-SiO_2 particles are poorly bonded with RC (Scheme 2). Thus, the film with optimum nano-SiO_2 loading (1–3 wt%) shows better impermeability to moisture. These results indicated that the addition of 2 or 3 wt% of nano-SiO_2 is optimal to produce composite films with the lowest WVP. Comparable optimum

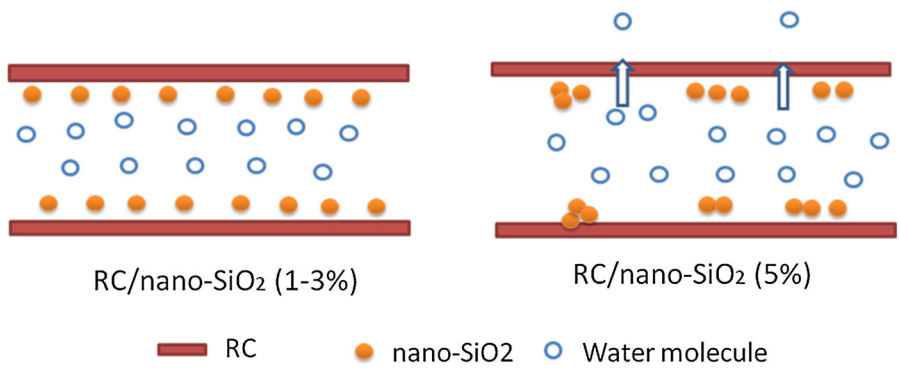

Scheme 2 Schematic representation of water vapor permeability of RC/nano-SiO_2

concentrations of nanofillers have been often reported for other types of nanofillers such as clay (Farahani et al. 2015). Farahani et al. observed a similar behavior for RC/nanoclay films. Rhim (2011) confirmed the effect of MMT clay (Cloisite Na^+) content on the film properties of agar/clay nanocomposite films and revealed that the addition of 5 wt% nanoclay was the most effective for decreasing the WVP of the nanocomposite film, compared to higher concentrations of nanoclay.

Moisture content and water contact angle

The effects of nano-SiO_2 on the moisture contents of the composite films are summarized in Table 3. The experimental results indicated that the inclusion of nano-SiO_2 reduces moisture absorption, signifying that water has less affinity with the reinforced films. With the addition of nano-SiO_2, a stronger interaction occurs between nano-SiO_2 and RC than between RC and water. The number of hydrophilic sites for water molecules decreases by the formation of strong bonds between the RC matrix and nano-SiO_2, reducing the moisture content in the RC/nano-SiO_2 composite films.

The surface hydrophobicity and wettability of the polymer films can be assessed by their CAs, as shown in Table 3. The surface hydrophobicity of the RC/nano-SiO_2 composite films is slightly higher than that of neat RC film. The increment in the CA indicates a good interaction between nano-SiO_2 and RC. The higher CA of the nanocomposite film could be ascribed to the higher hydrophobicity of nano-SiO_2 than that of the RC biopolymer. Similar results were obtained with the insertion of MMT clay in RC nanocomposite films (Mahmoudian et al. 2012).

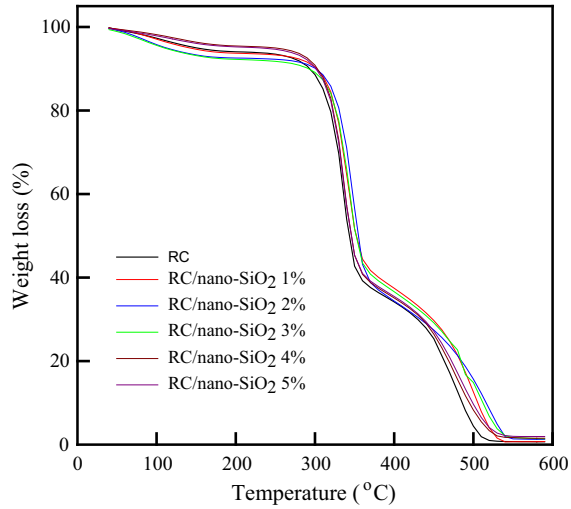

Fig. 4 Primary thermograms of RC film and RC/nano-SiO_2 composite films

Thermal properties

The thermal stabilities of the RC film and RC/nano-SiO_2 composite films were evaluated by TGA, and the primary thermograms and results are shown in Fig. 4 and Table 4. T_{10}, T_{20}, and T_{50} respectively represent the temperatures at which 10, 20, and 50% weight loss occur. The TGA thermograms of RC film and RC/nano-SiO_2 composite films showed three distinctive weight loss regimes; at 80–150 °C by the evaporation of unbound and bound water molecules, at 250–350 °C by a significant decomposition of cellulose, and at 350–450 °C by the carbonization of cellulose, respectively.

In general, the thermal stability of the RC film is increased with the reinforcement of the film with nano-SiO_2 as deduced by the observed T_{10}, T_{20}, and T_{50} values of the neat RC film. Further, it is observed

Table 4 Thermal degradation parameters of RC film and RC/nano-SiO_2 composite films

Sample code	T_{10} (°C)	T_{20} (°C)	T_{50} (°C)	Char content (%)
RC	281 ± 2.7	312 ± 8.1	339 ± 2.3	0.92 ± 0.1
RC/nano-SiO_2 1%	306 ± 2	329 ± 1.2	354 ± 1.8	1.31 ± 0.4
RC/nano-SiO_2 2%	309 ± 2.9	335 ± 2.6	359 ± 1.7	1.92 ± 0.6
RC/nano-SiO_2 3%	296 ± 3	331 ± 2.7	357 ± 2.4	2.2 ± 0.7
RC/nano-SiO_2 4%	304 ± 3.5	326 ± 3.2	350 ± 2.8	2.65 ± 0.8
RC/nano-SiO_2 5%	305 ± 2.6	327 ± 1.7	349 ± 2.2	3.6 ± 1.1

T_{10}, T_{20} and T_{50} represent the temperature occurred at weight loss of 10, 20 and 50%, respectively

that the thermal stability increase is limited only up to 3 wt% of the added nano-SiO_2. In other words, there is no significant increment in the onset and other thermal decomposition temperatures of the RC/nano-SiO_2 films with 4 and 5 wt% of nano-SiO_2 content. The increments in the thermal stabilities of the RC/nano-SiO_2 composite films are due to the obstruction of volatile mass transfer to the surface by the nanoparticles (outmigration of degraded volatiles) which retards the decomposition rate. In general, the increase in the degradation temperature of polymer/MMT nanocomposites was also attributed to the good dispersion and exfoliation of MMT in the polymer matrix (Ray and Bousmina 2005). In the present study, agglomeration is observed (by SEM) at higher loadings of nano-SiO_2 in the composite films, in which the dispersion of the filler is non-uniform. Particle agglomeration reduces the nano-SiO_2 surface area available for char formation; therefore, the thermal stability of the nanocomposite is reduced. Delhom et al. (2010) also reported a decrease in the degradation temperatures of cotton/MMT nanocomposites at higher contents of MMT.

The char yields at 600 °C for neat RC film and RC/nano-SiO_2 composite films are also shown in Table 4. The char yield is higher for the RC/nano-SiO_2 nanocomposite films compared to that of neat RC film and increases with increasing loading of nano-SiO_2. The residual char is attributed to the relatively higher thermal stability of nano-SiO_2 (Ray and Bousmina 2005).

In addition to TGA, DSC was performed to understand the decomposition temperatures of neat RC film and RC/nano-SiO_2 composite films (Fig. 5). Two exothermic peaks at ~ 350 and ~ 450 °C, indicating the thermal-oxidative degradation of the

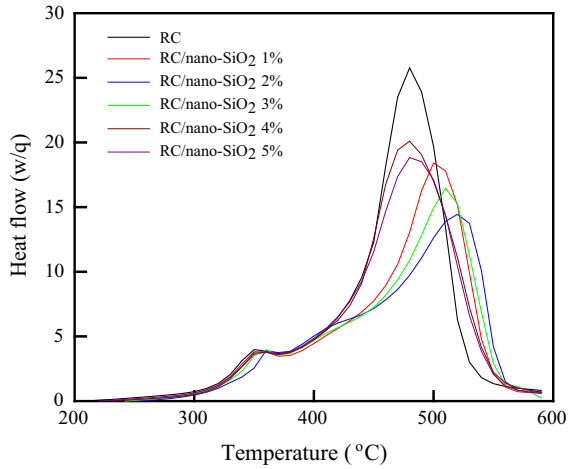

Fig. 5 DSC curves of RC film and RC/nano-SiO_2 composite films

composite films, are apparently observed (Delhom et al. 2010). The cellulose decomposition temperature of neat RC film is increased from 356 to 365 °C upon the addition of nano-SiO_2 (2 wt%) and there is no significant change further loading of nano-SiO_2. Compared to that of neat RC film, the thermal decomposition process is retarded for all the RC/nano-SiO_2 composite films, suggesting the increased stabilities of the composite films. This may be due to the high thermal stability of the nano-SiO_2 particles in the film along with their good dispersion in the RC matrix. These results are consistent with those reported by us for RC/MMT clay nanocomposites (Cerruti et al. 2008); in the presence of nanoclay, thermal transfer was retarded and oxygen diffusion into the polymer bulk was hindered. Therefore, in the present case, it is speculated that the oxidative reaction could be stabilized for the nanocomposite films,

because of the thermally stable nano-SiO_2 particles. Further, higher loading of nano-SiO_2 leads to low thermal-oxidative temperatures due to increased agglomeration.

Conclusions

A series of RC/nano-SiO_2 bionanocomposite films composed of regenerated cellulose (RC) and nano-sized SiO_2 particles of 20–40 nm was successfully prepared. The physical properties of the composite films were significantly influenced by the content of nano-SiO_2 particles. Nano-SiO_2 contents of $\sim$ 2 wt% resulted in improved tensile and thermal properties as well as water vapor barrier properties. FT-IR and SEM results indicated that strong molecular interactions occurred between RC and nano-SiO_2, promoting good dispersion in the RC matrix at low concentrations of nano-SiO_2. Lower moisture contents and higher water CAs indicated improved hydrophobicity of the RC/nano-SiO_2 composite films compared to neat RC film. Further, TGA revealed that the thermal stability of the RC/nano-SiO_2 composite films was higher than that of neat RC film. This study highlights the potential of organically modified nano-SiO_2 to enhance the properties of RC because of the ability of nano-SiO_2 to interact with the RC matrix at very low concentrations (2 wt%). This is expected to play a significant role in industrial applications, particularly in membrane technology and packaging.

Acknowledgments This work was supported by both the National Research Foundation of Korea (NRF) grant funded by the Korea government (MSIP) [No. 2017R1A2B4011234].

References

Ashok B, Reddy KO, Madhukar K, Cai J, Zhang L, Rajulu AV (2015) Properties of cellulose/*Thespesia lampas* short fibers bio-composite films. Carbohydr Polym 127:110–115

Bikiaris DN, Vassiliou A, Pavlidou E, Karayannidis GP (2005) Compatibilisation effect of PP-g-MA copolymer on iPP/SiO_2 nanocomposites prepared by melt mixing. Eur Polym J 41:1965–1978

Boissiere C, Kummel M, Persin M, Larbot A, Prouzet E (2001) Spherical MSU-mesoporous silica particles tuned for HPLC. Adv Funct Mater 11:129–135

Cai J, Zhang L, Chang C, Cheng G, Chen X, Chu B (2007a) Hydrogen-bond-induced inclusion complex in aqueous cellulose/LiOH/urea solution at low temperature. ChemPhysChem 8:1572–1579

Cai J, Zhang L, Zhou J, Qi H, Chen H, Kondo T, Chen X, Chu B (2007b) Multifilament fibers based on dissolution of cellulose in NaOH/urea aqueous solution: structure and properties. Adv Mater 19:821–825

Cerruti P, Ambrogi V, Postiglione A, Rychly J, Matisová-Rychla L, Carfagna C (2008) Morphological and thermal properties of cellulose–montmorillonite nanocomposites. Biomacromolecules 9:3004–3013

Dai TY, Wang HJ, Cao Y (2015) Preparation, characterization and application of polyaniline/epoxide polysiloxane composite films. Chin J Polym Sci 33:732–742

Delhom CD, White-Ghoorahoo LA, Pang SS (2010) Development and characterization of cellulose/clay nanocomposites. Compos B Eng 41:475–481

Farahani MF, Bedane AH, Pan Y, Xiao H, Eic M, Chibante F (2015) Cellulose/nanoclay composite films with high water vapor resistance and mechanical strength. Cellulose 22:3941–3953

Gennadios A, Weller CL, Goodings CH (1994) Measurement errors in water vapor permeability of high permeable hydrophilic edible films. J Food Eng 21:395–409

Grun M, Lauer I, Unger KK (1997) The synthesis of micrometer- and submicrometer-size spheres of ordered mesoporous oxide MCM-41. Adv Mater 9:254–257

Han D, Yan L, Chen W, Li W, Bangal PR (2011) Cellulose/graphite oxide composite films with improved mechanical properties over a wide range of temperature. Carbohydr Polym 83:966–972

Jayaramudu J, Reddy GSM, Varaprasad K, Sadiku ER, Ray SS, Rajulu AV (2013) Preparation and properties of biodegradable films from *Sterculia urens* short fiber/cellulose green composites. Carbohydr Polym 93:622–627

Khalil HPS, Abdul AH, Bhat AF, Ireana Y (2012) Green composites from sustainable cellulose nanofibrils: a review. Carbohydr Polym 87:963–979

Kim DH, Park SY, Kim J, Park M (2010) Preparation and properties of the single-walled carbon nanotube/cellulose nanocomposites using *N*-methylmorpholine-*N*-oxide monohydrate. J Appl Polym Sci 117:3588–3594

Klemm D, Heublein B, Fink HP, Bohn A (2005) Cellulose: fascinating biopolymer and sustainable raw material. Angew Chem Int Ed 44:3358–3393

Lagaron JM, Catalá R, Gavara R (2004) Structural characteristics defining high barrier polymeric materials. Mater Sci Technol 20:1–7

Lai SM, Hsieh YT (2016) Preparation and properties of polylactic acid (PLA)/silica nanocomposites. J Macromol Sci Part B 55:211–228

Li J, Wei X, Wang Q, Chen J, Chang G, Kong L, Su J, Liu Y (2012) Homogeneous isolation of nanocellulose from sugarcane bagasse by high pressure homogenization. Carbohydr Polym 90:1609–1613

Mahmoudian S, Wahit MU, Ismail AF, Yussuf AA (2012) Preparation of regenerated cellulose/montmorillonite nanocomposite films via ionic liquids. Carbohydr Polym 88:1251–1257

Mohammad S, Mat UW, Shaya M, Nurbaiti AH (2013) Regenerated cellulose/halloysite nanotube nanocomposite

films prepared with an ionic liquid. Mater Chem Phys 141:936–943

Mohammad S, Mat UW, Abdirahman AY, Al-Saleh MA, Wong TW (2014) Characterization of bio regenerated cellulose/sepiolite nanocomposite films prepared via ionic liquid. Polym Test 33:121–130

Moon RJ, Martini A, Nairn J, Simonsenf J, Youngblood J (2011) Cellulose nanomaterials review: structure, properties and nanocomposites. Chem Soc Rev 40:3941–3994

Nadhan AV, Rajulu AV, Li R, Cai J, Zhang L (2012) Properties of waste silk short fiber/cellulose green composite films. J Compos Mater 46:123–127

Pasternack RM, Sandrine RA, Yves JC (2008) Attachment of 3-(aminopropyl) triethoxysilane on silicon oxide surfaces: dependence on solution temperature. Langmuir 24:12963–12971

Qi H, Chang C, Zhang L (2009) Properties and applications of biodegradable transparent and photoluminescent cellulose films prepared via a green process. Green Chem 11:177–184

Qi H, Liu J, Gao S, Mader E (2013) Multifunctional films composed of carbon nanotubes and cellulose regenerated from alkaline–urea solution. J Mater Chem A 1:2161

Rahatekar SS, Rasheed A, Jain R, Zammarano M, Koziol KK, Windle AH, Gilman JW, Kumar S (2009) Solution spinning of cellulose carbon nanotube composites using room temperature ionic liquids. Polymer 50:4577–4583

Ray S, Bousmina M (2005) Biodegradable polymers and their layered silicate nanocomposites: in greening the 21st century materials world. Prog Mater Sci 50:962–1079

Reddy JP, Rhim JW (2014) Characterization of bionanocomposite films prepared with agar and paper-mulberry pulp nanocellulose. Carbohydr Polym 110:480–488

Rhim JW (2011) Effect of clay contents on mechanical and water vapor barrier properties of agar-based nanocomposite films. Carbohydr Polym 86:691–699

Rhim JW, Wang LF (2013) Mechanical and water barrier properties of agar/-carrageenan/konjac glucomannan ternary blend biohydrogel films. Carbohydr Polym 96:71–81

Saravanan S, Akshay Gowda KM, Ramamurthy PC, Giridhar M (2016) Influence of mesoporous silica and butyral content on the mechanical, water absorption, and permeability properties of in situ synthesized silica/PVB nanocomposite films. Polym Plast Technol Eng 55:1220–1230

Soheilmoghaddam M, Wahit MU, Whye WT, Akos NI, Pour RH, Yussuf AA (2014) Bionanocomposites of regenerated cellulose/zeolite prepared using environmentally benign ionic liquid solvent. Carbohydr Polym 106:326–334

Song H, Zheng L (2013) Nanocomposite films based on cellulose reinforced with nano-SiO2: microstructure, hydrophilicity, thermal stability, and mechanical properties. Cellulose 20:1737–1746

Tang XZ, Kumar P, Alavi S, Sandeep KP (2012) Recent advances in biopolymers and biopolymer-based nanocomposites for food packaging materials. Crit Rev Food Sci Nutr 52:426–442

Thomas JM, Johnson BFG, Raja R, Sankar G, Midgley PA (2003) High-performance nanocatalysts for single-step hydrogenations. Acc Chem Res 36:20–30

Tsioptsias C, Panayiotou C (2008) Preparation of cellulose–nanohydroxyapatite composite scaffolds from ionic liquid solutions. Carbohydr Polym 74:99–105

Vladimirov V, Betchev C, Vassiliou A, Papageorgiou G, Bikiaris D (2006) Dynamic mechanical and morphological studies of isotactic polypropylene/fumed silica nanocomposites with enhanced gas barrier properties. Compos Sci Technol 66:2935–2944

Yan S, Yin J, Yang Y, Dai Z, Ma J, Chen J (2007) Surface-grafted silica linked with l-lactic acid oligomer: a novel nanofiller to improve the performance of biodegradable poly(l-lactide). Polymer 48:1688–1694

Yang Q, Qi H, Lue A, Hu K, Cheng G, Zhang L (2011) Role of sodium zincate on cellulose dissolution in NaOH/urea aqueous solution at low temperature. Carbohydr Polym 83:1185–1191

Zha J, Lu X, Xin Z (2015) A rational design of double layer mesoporous polysiloxane coatings for broadband antireflection. J Sol Gel Sci Technol 74:677–684

Zhang H, Guo L, Shao H, Hu X (2006) Nano-carbon black filled lyocell fiber as a precursor for carbon fiber. J Appl Polym Sci 99:65–74

Zhang H, Wang ZG, Zhang ZN, Wu J, Zhang J, He JS (2007) Regenerated-cellulose/multiwalled-carbon-nanotube composite fibers with enhanced mechanical properties prepared with the ionic liquid 1-allyl-3-methylimidazolium chloride. Adv Mater 19:698–704

Zhu A, Diao H, Rong Q, Cai A (2010) Preparation and properties of polylactide–silica nanocomposites. J Appl Polym Sci 116:2866–2873

Zou H, Wu S, Shen J (2008) Polymer/silica nanocomposites: preparation, characterization, properties, and applications. Chem Rev 108:3893–3957